Published in final edited form as:
Eur J Neurosci. 2014 February ; 39(4): 593–601. doi:10.1111/ejn.12418.

Spatiotemporal flow of information in the early visual pathway

Bartlett D. Moore IV[1,2], **Daniel L. Rathbun**[3,4], **W. Martin Usrey**[4], and **Ralph D. Freeman**[1]

[1]Vision Science Group, Helen Wills Neuroscience Institute and School of Optometry, University of California, Berkeley, 360 Minor Hall, Berkeley, CA 94720-2020, USA

[2]Center for Mind and Brain, University of California, Davis, Davis, CA, USA

[3]Center for Integrative Neuroscience, University of Tuebingen, Germany

[4]Center for Neuroscience, University of California, Davis, Davis, CA, USA

Abstract

The spatial components of a visual scene are processed neurally in a sequence of coarse features followed by fine features. This coarse-to-fine temporal stream was initially considered to be a cortical function, but has recently been demonstrated in the dorsal lateral geniculate nucleus. The goal of this study was to test the hypothesis that coarse-to-fine processing is present at earlier stages of visual processing in the retinal ganglion cells that supply lateral geniculate nucleus (LGN) neurons. To compare coarse-to-fine processing in the cat's visual system, we measured the visual responses of connected neuronal pairs from the retina and LGN, and separate populations of cells from each region. We found that coarse-to-fine processing was clearly present at the ganglion cell layer of the retina. Interestingly, peak and high-spatial-frequency cutoff responses were higher in the LGN than in the retina, indicating that there was a progressive cascade of coarse-to-fine information from the retina to the LGN to the visual cortex. The analysis of early visual pathway receptive field characteristics showed that the physiological response interplay between the center and surround regions was consistent with coarse-to-fine features and may provide a primary role in the underlying mechanism. Taken together, the results from this study provided a framework for understanding the emergence and refinement of coarse-to-fine processing in the visual system.

INTRODUCTION

Spatial processing in the central visual pathway generally occurs in a temporal sequence in which large-scale features are followed by those of a finer nature (Hegde, 2008). This sequence of coarse-to-fine processing was initially thought to be a function of the visual cortex (Ringach *et al.*, 1997; Mazer *et al.*, 2002; Shapley *et al.*, 2003). However, recent work demonstrates that it is clearly present at the level of the lateral geniculate nucleus (LGN) (Allen & Freeman, 2006). A coarse-to-fine processing system was initially postulated in a theoretical approach (Marr, 1982). It has also been demonstrated for spatial frequency (SF) analysis both behaviorally (McSorley & Findlay, 1999) and neurophysiologically (Bredfeldt & Ringach, 2002; Nishimoto *et al.*, 2005) for orientation

Correspondence: Ralph D. Freeman, Vision Science Group, Helen Wills Neuroscience Institute and School of Optometry, University of California, Berkeley, 360 Minor Hall, Berkeley, CA 94720-2020, USA rfreeman@berkeley.edu.

and direction selectivity (Ringach *et al.*, 1997; Pack & Born, 2001; Mazer *et al.*, 2002), stereoscopic depth processing in the visual cortex (Menz & Freeman, 2003) and somatosensory (Sripati *et al.*, 2006) and oculomotor (Over *et al.*, 2007) systems. Considered together, these findings suggest that coarse-to-fine processing is a basic and general feature of neural circuitry.

Here, we explore the hypothesis that coarse-to-fine processing is initiated at first-order neurons in the visual pathway. Although it may be inferred that this processing strategy originates in the retina, this possibility has not been verified. If present in the retina, an important question to address is whether there is a relationship between the time-course and magnitude of coarse-to-fine processing and the spatiotemporal profile of retinal center/surround receptive fields (RFs), as the larger and delayed antagonistic surrounds of retinal RFs are thought to contribute to the attenuation of retinal responses to visual stimuli containing low SFs (Baylor *et al.*, 1971b; Enroth-Cugell *et al.*, 1983; Mastronarde, 1987b; Usrey *et al.*, 1999; Ruksenas *et al.*, 2000; Flores-Herr *et al.*, 2001). Along these lines, the relatively stronger surrounds of LGN RFs may underlie a cascading increase or progressive shift in coarse-to-fine processing as visual signals are processed *en route* from the retina to the cortex. To test the predictions, we carry out neurophysiological studies of three populations of neurons. The first population consists of pairs of connected retinal ganglion cells and LGN neurons. All cell pairs in this population have overlapping RFs and cross-correlograms indicating that they are monosynaptically connected. The second and third groups of cells are independent populations of retinal ganglion cells and LGN neurons.

To carry out the required analysis, we obtain spatiotemporal RF maps of simultaneously recorded pairs of connected retinal ganglion cells and LGN cells. We then analyze the RF spectrotemporal dynamics to obtain comparisons of timing of RF subunits. We also perform the same analysis for the separate populations of retinal ganglion cells and LGN neurons.

Our primary finding is that coarse-to-fine processing is robust in retinal ganglion cells and LGN neurons. In addition, our analysis supports the view that the temporal characteristics of RF surround responses in the retina and LGN play an essential role in the tuning of coarse-to-fine processing. Although cells in the LGN are classically considered to have more pronounced center-surround interactions compared with those of the retina, this interaction does not appear to influence all aspects of coarse-to-fine processing, as we do not find significant differences between the retina and LGN in absolute ranges or temporal sequences of coarse-to-fine processing, but do find significantly higher mean peak and high-cutoff SF levels in the LGN compared with the retina. These latter results demonstrate a temporal cascade of spatial information processing from the retina to the LGN to the visual cortex.

Materials and methods

Animal preparation

The surgical and experimental procedures conformed to NIH guidelines and were approved by the University of California Animal Care and Use Committee. Mixed-breed mature cats (University of California, Davis colony) were initially anesthetized with ketamine (10 mg/kg, i.m.) or isoflurane and maintained with thiopental sodium (10-20 mg/kg, i.v.,

supplemented as needed). Animals were placed in a stereotaxic apparatus and mechanically respired with a 2 : 1 mixture of oxygen and nitrous oxide. The electrocardiogram, electroencephalogram, and expired CO_2 levels were continuously monitored and body temperature was maintained at 38 °C. The animals were paralyzed with vecuronium bromide (0.2 mg/kg/h, i.v.) to prevent eye movements. Anesthesia was maintained with thiopental sodium at rates determined individually for each animal (1-3 mg/kg/h, i.v.). An appropriate level of anesthesia was ensured throughout each experiment by (i) monitoring the electroencephalogram for changes in slow-wave/spindle activity and (ii) monitoring the electrocardiogram and expired CO_2 for changes associated with a decrease in the depth of anesthesia. If any of these measures indicated a decrease in the depth of anesthesia, the delivery of thiopental sodium was increased. Pupils were dilated and nictitating membranes were retracted. The eyes were fitted with contact lenses.

Electrophysiological recording

Single-cell recordings were conducted either simultaneously from retinal ganglion cells and neurons in the LGN or from separate populations at each location. Retinal recordings were made intraocularly. Intraocular retinal recordings were made using a custom-fabricated tungsten-in-glass microelectrode. The electrode was introduced through the sclera into the posterior chamber of the eye through a guide tube and positioned using a micromanipulator. LGN units in layer A were recorded with a single electrode or a multielectrode array consisting of seven electrodes (concentric arrangement; 1 MΩ impedance) that could be independently raised and lowered (Thomas Recording, Marburg, Germany) (Eckhorn and Thomas, 1993). The LGN electrodes were typically positioned first, after which a small spot of light was then used to locate the region of the retina that was excitatory for the LGN neurons. This region was then targeted for the retinal recordings. Spike isolation was performed online and offline using waveform analysis, the presence of a refractory period in the autocorrelogram and, in some cases, parametric cluster analysis. The responses were amplified, band-pass filtered between 10 Hz and 10 kHz, and recorded at 28 kHz on a computer equipped with a Power 1401 data acquisition interface and Spike 2 software (Cambridge Electronic Design, Cambridge, UK).

A spatiotemporal binary white-noise stimulus was used to map retinal and geniculate RFs (Sutter, 1987; DeAngelis *et al.*, 1993a,b; Reid *et al.*, 1997; Usrey & Reid, 1999; Rathbun *et al.*, 2010). In some cases, separate sine-wave grating stimuli were used to collect large numbers of spikes for cross-correlation analysis and to distinguish X and Y cell types. Visual stimuli were created with a VSG2/5 (Cambridge Research Systems, Rochester, UK) and presented on a gamma-calibrated Sony Artisan display running at 140 Hz. The mean luminance of the display was 38 candelas/m^2.

Assessment of synaptic connectivity

The connectivity between retinal and LGN cells was assessed by cross-correlation of retinal and LGN spike trains. Using a bin duration of 100 μs, a short-latency peak (~2–6 ms offset from zero) in the cross-correlogram was taken as evidence of a monosynaptic connection between cell pairs (Mastronarde, 1987a,b; Usrey & Reid, 1999; Usrey *et al.*, 1999; Rathbun *et al.*, 2010). Once the bin containing the peak was identified, all neighboring bins with

values greater than 3 SDs above the baseline mean were considered part of the peak. The baseline mean was calculated using bins from 30 to 50 ms on either side of the peak bin. A significant correlation was indicative of a direct connection between a retinal ganglion cell and an LGN neuron. The connection strength was quantified as the integral of the correlogram peak normalized by the total number of geniculate (postsynaptic) spikes. This value therefore represented the fraction of the geniculate spikes that were caused by a spike from the retinal neuron (Levick *et al.*, 1972; Usrey *et al.*, 1998; 1999; Rathbun *et al.*, 2010).

Receptive field analysis

Spatiotemporal RFs were mapped via reverse-correlation analysis using a pseudorandom binary white-noise checkerboard stimulus (Jones & Palmer, 1987; DeAngelis *et al.*, 1993a,b; Reid *et al.*, 1997; Usrey & Reid, 1999; Usrey *et al.*, 1999). For each temporal delay between stimulus and response, we calculated the average stimulus that preceded a spike. The resulting spatiotemporal RF map can be thought of as the average firing rate of the neuron, above or below the mean, for each pixel in the stimulus (the impulse response). Impulse responses were calculated for both RF center and surround subunits, and interpolated separately with a cubic spline function. The RF center was defined as all contiguous spatial positions having the same sign at the strongest response and 1.5 SD above the baseline noise value. The surround was defined as all other positions within three radius values of the center. The strength of the center and surround subunits at each time-point was defined as the amplitude of the respective impulse responses.

For most cells, we used a null test (Enroth-Cugell and Robson, 1966, Hochstein and Shapley, 1976; Usrey et al., 1999) with a contrast-reversing grating to distinguish X and Y cell types (NB W cells were not present in layer A). For some cells, we compared RF sizes to differentiate X and Y cells recorded concurrently (Linsenmeier *et al.*, 1982).

Spatial frequency tuning analysis

To evaluate the SF, we interpolated the RF across X and Y dimensions and integrated over the Y dimension. Spectrotemporal RFs with two dimensions, SF and time, were obtained via Fourier transforms performed in MATLAB (The Mathworks, Natick, MA, USA). We restricted our analysis to the first phase of the response by setting a temporal analysis window with initial and final time-points. This temporal window was defined as the interval between which the energy of the spectrotemporal RF reached and decayed to half-maximum. This window was selected because it successfully isolated the initial RF response phase in an unbiased and reliable manner.

To characterize the SF dynamics, we calculated the peaks and bandwidths. We fit each slice of the spectrotemporal RF to a difference of Gaussians function. The optimal SF (SF_{peak}) is the maximum point in this function. The high cutoff SF (SF_{high}) is the SF at which the tuning curve decreased to half-maximum. The bandwidth at each time-point is defined as the log ratio of SF_{high} to SF_{peak}

$$bw(t)=\log_2\left(\frac{SF_{high}(t)}{SF_{peak}(t)}\right)$$

where SF_{high} is the half-maximum SF on the rising side of the tuning curve. The change in SF_{peak} within the analysis window is quantified as the log ratio of the final SF to the initial SF

$$\Delta SF_{peak}=\log_2\left(\frac{SF_{peak}(t_{final})}{SF_{peak}(t_{initial})}\right)$$

The change in the tuning is quantified as the difference between the final and initial bandwidths: $\Delta bw = bw(t_{final}) - bw(t_{initial})$.

This analysis window adequately captures the increase in peak SF and the decrease in tuning width during the first phase of the response. A broader analysis window is necessary to compare the timing of SF tuning with dynamic RF center and surround strengths. We defined an additional interval to compare these features as described previously (Allen & Freeman, 2006). The initial time-point in this window was set as the time where the two-dimensional RF variance first exceeded a threshold of 5 SDs above the baseline mean. The final time-point was the time at which the SD of the two-dimensional STRF first fell below this threshold. The statistical comparisons were performed using non-parametric methods.

RESULTS

We made extracellular recordings of visually evoked responses from retinal ganglion cells and LGN neurons in the cat in an effort to determine the origin and underlying mechanisms of coarse-to-fine processing in the early visual system. To obtain spatiotemporal RF maps for each cell under study, we used a binary white-noise stimulus with reverse correlation analysis as described in previous work (Jones & Palmer, 1987; Jones *et al.*, 1987; DeAngelis *et al.*, 1993a,b; Reid *et al.*, 1997; Usrey *et al.*, 1999; Rathbun *et al.*, 2010). This process yielded two dimensions of space and one of time as illustrated in the cube of Fig. 1A. Here, different time delays between spikes and stimuli are shown for two-dimensional spatial noise stimuli, which results in a three-dimensional analysis. Figure 1B represents spike trains from retinal ganglion cells and LGN neurons that occur during simultaneous recordings at the two sites. The retinal spike rates were higher than those of the LGN, which is typical of previous studies (Usrey et al, 1999; Rathbun et al. 2010). A cross-correlogram of spike discharge from the two regions is depicted in Fig. 1C for simultaneous recordings. The prominent peak at around 3 ms was used in the identification of neurally connected pairs of cells (Mastronarde, 1987a,b; Reid & Alonso, 1995; Usrey & Reid, 1999; Usrey *et al.*, 1999). Within the XYT cube of Fig. 1D is a two-dimensional spatial RF map at a given time. Similar maps may be shown for different values of T. For a complete map over time, the cube was integrated along the Y axis, which resulted in a space time (XT) plot as shown at the bottom of Fig. 1D. Bright and dark excitatory (ON and OFF) regions are represented, respectively, by red and blue areas. The XY plot of Fig. 1D, which is for a retinal ganglion

cell, is reproduced in Fig. 1E. A similar plot is shown in Fig. 1F for an LGN neuron that is functionally connected to the retinal cell depicted in Fig. 1E. The RF profiles of these two cells were similar, but the center was weaker and more elongated in space for the LGN neuron. For a complete set of times, XT plots may be derived for these two cells, and they are depicted in Fig. 1G and H.

The SF was central to our analysis, and it may be derived from our spatiotemporal RF maps. We computed Fourier transforms at each time-point to obtain SF time plots. This was a standard procedure and the results agreed well with values derived from measurements with sine-wave gratings (Jones & Palmer, 1987; DeAngelis *et al.*, 1993a,b; Allen & Freeman, 2006). Examples of this transformation are shown for a pair of connected retinal ganglion and LGN cells in Fig. 2. The spatiotemporal maps are shown in Fig. 2A and B and their equivalent spectrotemporal plots are given in Fig. 2C and D, respectively. In both cases, the SF plots are slightly tilted in time in a rightward direction and the second phases are similar but much weaker. We limited our current analysis to first-phase values, which were nearly always relatively strong.

To evaluate coarse-to-fine processing, we focused on SF tuning and how it may change during responses. We used the SF peak, i.e. optimal or preferred, high cutoff, and bandwidth values to estimate tuning changes during responses. With this analysis, neurons with coarse-to-fine processing were expected to show an initial response (selectivity) to stimuli with low SFs and subsequent responses to stimuli containing higher SFs. Moreover, depending on the time-course of low-frequency attenuation and high-frequency growth, the bandwidth for SF tuning would be expected to broaden, narrow, or remain the same over the visual response. The optimal SF tuning for each time-point of the response was estimated by fits of SF profiles with difference of Gaussian functions. We then defined a specific temporal interval during the first phase of the response. Arbitrarily, we used the first point in the interval to represent the time at which energy in the spectrotemporal RF first reached a half-maximum value t_{initial}. Similarly, we considered the endpoint to be the time at which energy was first decreased to a half-maximum value t_{final}. These initial and final time-points are indicated by downward arrows in Fig. 2E and F. The dotted sections of the curves in Fig. 2E and F represent changes in the peak SF during the full initial phase of the RF. In addition to the peak SF, we also estimated the cutoff SF, for which values are shown in subsequent figures. The other relevant variable was the SF bandwidth to determine if the tuning changed as the peak SF increased. For the examples in Fig. 2, the bandwidth decreased substantially during the analysis time window as shown in Fig. 2G and H. The higher selectivity for SF was clearly correlated with the increased peak values of Fig. 2E and F.

To investigate the potential mechanisms of observed SF changes, we examined the time-course and strength of center and surround RF components, as the interplay between the center and surround probably provided a substrate for coarse-to-fine processing. For the retina and LGN representative cells of Fig. 2, we show normalized response functions in Fig. 2I and J for center (red) and surround (blue) components. Note that the profiles are nearly symmetrically opposite during the first prominent phase of the response. As expected, the surround responses were delayed in time with respect to those of the center, and the profiles were similar for the retina and LGN. However, there was a slightly greater temporal

difference between the center and surround peak values in the case of the LGN example. The change in relative surround strength is indicated for both cells in Fig. 2K and L. The relative surround strength was calculated as the ratio between the strength of the surround and that of the center at each time-point. A surround-center ratio of 1 indicated that the two subunits were balanced in strength. The surround strength increased during the first phase of the response for both cells, but the LGN surround was stronger at t_{final}.

In order to gain a better understanding of the range of responses that existed between monosynaptically connected retinal ganglion cells and LGN neurons, we extended the comparisons of SF levels to our entire sample of connected cell pairs. In Fig. 3A, peak mean SF values are compared for the LGN (ordinate) and retinal ganglion cells (abscissa). The values were calculated from integration of the initial phases of spectrotemporal RF data as follows. For each cell, we integrated the spectrotemporal RF between $t_{initial}$ and t_{final} to determine the average peak SF. Separate sets of data are shown for relatively strong (filled circles) or weak (open circles) connection strengths for each pair of cells. The connection strength was determined by the proportion of LGN spikes that were preceded by a retinal spike, as described in Materials and methods. For these and subsequent figures, cell pairs with a connection strength above the population median (0.154) are depicted by filled circles. Pairs with connection strengths below the median are depicted by open circles. Most data points in Fig. 3A fall above the Y=X line, showing that LGN cells generated higher SF peaks compared with their retinal afferent inputs. The difference was significant ($p < 0.05$, one-tailed Wilcoxon rank-sum test). The data in Fig. 3B are analogous to those in Fig. 3A, but they compare retina and LGN cells in terms of high SF cutoff values. As in Fig. 3A, most of the data points are above the diagonal 1 : 1 line, which again demonstrates that LGN cells generally have relatively higher SF cutoff values. This was also statistically significant ($p < 0.05$, one-tailed Wilcoxon rank-sum test). In addition to response levels, the SF tuning characteristics were also relevant. The plot in Fig. 3C compares LGN and retinal bandwidth. The data are distributed more evenly than in the previous two cases, but LGN cells have slightly higher selectivity (lower bandwidth) compared with those of the retina ($p < 0.05$, one-tailed Wilcoxon rank-sum test). When the data were separated into categories of weak and strong connection strengths, the results were similar to those for all data combined.

Having established that coarse-to-fine SF processing began in the retina, we now compared this sequence with that of neurons in the next stage, i.e. the LGN. The SF dynamic shift ranges are compared for coupled retina and LGN cell pairs in Fig. 4. Again, as in Fig. 3, relatively strong and weak intercellular connections are depicted, respectively, by filled and open circles. In Fig. 4A, a wide distribution is shown of degrees of SF peak shifts, and there is no obvious difference between relatively strong and weak connections. In contrast, the data in Fig. 4B, for high cutoff SF values, are clumped together in a relatively tight distribution. As in Fig. 4A, all but one cell show dynamic positive SF shifts. In spite of the difference in distributions between Fig. 4A and B, the shift magnitudes for the retina and LGN were similar (SF peak shifts: $p= 0.13$; high cutoff SF values: $p=0.32$; one-tailed Wilcoxon rank-sum test). In Fig. 4C, shifts in SF tuning are shown in terms of bandwidth for cell pairs. Once again there is a relatively wide distribution of values, but only one data point is in the positive part of the field, i.e. tuning bandwidth generally decreased during

positive SF shifts. Shifts in tuning bandwidth were similar between the retina and LGN (p=0.22, one-tailed Wilcoxon rank-sum test).

To assess the dynamic changes of individual monosynaptically coupled retina and LGN cell pairs, we plot peak SF changes at different times during responses in Fig. 5. Values for the retina (red lines) and LGN (green lines) cells from each of the pairs are represented for initial, intermediate and final SF peak values as a function of time during the response. The expected temporal difference between the retina and LGN response is represented by a small leftward displacement of the red lines compared with the green lines (Fig. 5A). Note that the slopes of all lines are tilted to the right, indicating a positive coarse-to-fine dynamic. Correspondingly, the bandwidth for the same cell pairs (Fig. 5B) is tilted to the left, demonstrating that SF tuning resolution becomes finer during responses. The slopes for both SF and bandwidth in Fig. 5A and B are not significantly different for the retina and LGN (p=0.84, t-test, and p=0.21, Wilcoxon rank-sum test, respectively). Mean values for connected cell pairs for peak SF and bandwidth are shown in Fig. 5C and D. The retina and LGN data are displaced in accordance with the time delay in transmission. The LGN cells had higher peak SF values at initial time-points than those of the retina and the difference was significant (0.05 ± 0.01 vs. 0.03 ± 0.01 c/d, respectively, $p<0.05$, one-tailed Wilcoxon rank-sum test). In addition, the mean LGN peak SFs at final time-points were higher than those of the retina but the difference was not significant (0.15 ± 0.01 vs. 0.13 ± 0.01 c/d, respectively, p=0.06, one-tailed Wilcoxon rank-sum test). As in Fig. 5B, the mean bandwidth changed over time (Fig. 5D), showing decreasing tuning widths during responses. When RFs began to emerge, the retina and LGN cells had similar bandwidths (4.1± 0.43 vs. 3.3 ± 0.44 octaves, respectively, p=0.09, one-tailed Wilcoxon rank-sum test). However, at the end of the first RF phase, LGN cells had relatively narrower bandwidth tuning (1.0 ± 0.01 vs. 1.2 ± 0.01 octaves, respectively, $p<0.01$, one-tailed Wilcoxon rank-sum test).

While in the process of searching for monosynaptically connected retinal ganglion cells and LGN neurons, we recorded the visual responses from a much larger sample of neurons in each structure, and the combined dataset (n=243; 52 RGCs, 191 LGN neurons) provided the basis for an extensive evaluation of coarse-to-fine processing across X and Y cell classes. Figure 6 shows summary data for SF shifts and changes in peak and cutoff SF values. In Fig. 6A, SF shifts are given for peak (shaded bars) and high cutoff (open bars) values for X and Y cells in retinal ganglion and LGN neurons. There were no statistically significant differences in the four values for peak or those for cutoff (peak= retinal X = 2.56 ± 0.66; retinal Y = 2.83 ± 0.37; LGN X = 2.90 ± 0.25; LGN Y = 3.19 ± 0.28; p= 0.25, one-tailed Wilcoxon rank-sum test; cutoff=retinal X = 0.044 ± 0.08; retinal Y = 0.58 ± 0.06; LGN X = 0.51 ± 0.03; LGN Y = 0.65 ± 0.05; p= 0.33, one-tailed Wilcoxon rank-sum test). Bandwidth values are compared for the same population of ganglion and LGN cells in Fig. 6B. Once again, there were no statistically significant differences although LGN cells tended to exhibit slightly higher levels of tuning, i.e. larger negative bandwidth shifts (retinal X = -2.12 ± 0.60; retinal Y = -2.25 ± 0.32; LGN X = -2.39 ± 0.22; LGN Y = -2.54 ± 0.26; p = 0.34, one-tailed Wilcoxon rank-sum test). Figure 6C shows mean SF peak (shaded bars) and high cutoff (open bars) values for the same four categories of neurons. Here, some important differences were evident as LGN cells showed higher mean SF values for both X and Y cells

(retinal X = 0.34 ± 0.04; retinal Y = 0.23 ± 0.02; LGN X = 0.42 ± 0.02; LGN Y = 0.31 ± 0.02; $p < 0.05$, one-tailed Wilcoxon rank-sum test). In addition, X cells exhibited higher mean SF values compared with those of Y neurons for both the retina and LGN, and again the difference was significant ($p < 0.01$, one-tailed Wilcoxon rank-sum test). The same trend held for high SF cutoffs (open bars), with significantly higher values for X cells compared with Y cells at both retinal and LGN levels ((retinal X = 0.89 ± 0.06; retinal Y = 0.60 ± 0.03; LGN X = 1.01 ± 0.02; LGN Y = 0.81 ± 0.03; $p < 0.05$, one-tailed Wilcoxon rank-sum test). The SF tuning bandwidths were similar in the retina and LGN and there were no overall statistically significant differences (retinal X = 1.48 ± 0.14; retinal Y = 1.69 ± 0.97; LGN X = 1.54 ± 0.07; LGN Y = 1.69 ± 0.10; $p = 0.06$, one-tailed Wilcoxon rank-sum test).

A functional basis of the SF characteristics that we have described above might be available from consideration of the internal structure of RFs in retina and LGN neurons. Classical descriptions indicate that most neurons in both areas exhibit center-surround RF organization, surround activity is temporally delayed with respect to that of the center, and RF surround strength is higher in the LGN compared with the retina (Kuffler, 1953; Hubel & Wiesel, 1961). We have analyzed temporal differences between center and surround RF components for our population of cells. In Fig. 7A, center-surround delay is plotted against peak SF shift for our entire population of cells for the same four categories displayed in Fig. 6. Filled circles and triangles represent, respectively, X and Y retinal ganglion cells. Open circles and triangles denote X and Y LGN neurons. The data for the retina and LGN are overlapped and there are no obvious differences. The data appear to constitute two separate distributions, and this is confirmed by Hartigans' dip test ($p<0.01$). The origin of this division is not clear and a least-squares fit to all of the data (dashed line) shows a positive correlation between center-surround delay and peak SF shift. The correlation was statistically significant for both retinal and LGN cells (retina: $r^2=0.13$, $p<0.05$; LGN: $r^2=0.09$, $p<0.05$). A similar comparison is made in Fig. 7B for center-surround delay vs. high SF cutoff shift. In this case, there is again overlap of data for the retina and LGN and the distribution appears homogeneous unlike that of Fig. 7A. This was confirmed statistically ($p=0.85$, Hartigans' dip test). There is again a positive correlation between delay and cutoff values, as shown by the dashed-line least-squares fit, which is statistically significant for LGN cells and nearly significant for the retinal population (retina: $r^2=0.07$, $p=0.054$; LGN: $r^2=0.03$, $p<0.05$). In Fig. 7C, center-surround delay is shown as a function of bandwidth shift for the same population of cells as in Fig. 7A. Once again, the apparent bimodal distribution is statistically confirmed ($p<0.01$, Hartigans' dip test). As expected, the increase in peak SF shift illustrated in Fig. 7A is accompanied by narrower bandwidth tuning in Fig. 7C. The least-squares fit for these data is again indicated by a dashed line. The negative correlation is statistically significant for both populations of cells (retina: $r^2=0.13$, $p<0.05$; LGN: $r^2=0.09$, $p<0.01$).

As there were clear differences in the temporal response properties of center and surround RF regions in the retina and LGN, it was of interest to examine these in relation to peak or preferred SF and bandwidth values. We have done this for our population of cells by considering SF values at times for which the response strength of center and surround RF activation was equal. In Fig. 7D, data are shown for the center surround balance points of retinal and LGN cells as a function of latencies to peak SF values. The data show a clear

positive correlation between these two variables, with nearly all of the data points falling above the Y=X line (retina: r^2=0.26, p<0.01; LGN: r^2=0.74, p<0.01). This means that peak SF values are reached slightly after time-points at which center and surround subunits have equal strengths and this is statistically significant (p<0.01, one-tailed Wilcoxon rank-sum test). A similar comparison is made in Fig. 7E for the same cells displayed in Fig. 7D for bandwidth change as a function of temporal center-surround balance. Again, there is a clear positive correlation between the variables (retina: r^2=0.34, p<0.01; LGN: r^2=0.76, p<0.01). Here, minimum bandwidth is attained slightly after time-points of equal center-surround subunit strengths as indicated by the preponderance of data above the Y=X line. This effect is statistically significant (p<0.01, one-tailed Wilcoxon rank-sum test). There are no obvious differences in these properties between the retina and LGN, and X and Y divisions. Considered together, these data are (i) consistent with a coarse-to-fine process in which peak or preferred resolution occurs just after the time at which center and surround strengths are balanced, and (ii) consistent with the hypothesis that center-surround neural circuits in the early visual pathways are linked to coarse-to-fine dynamic SF tuning.

DISCUSSION

We studied the coarse-to-fine processing sequence that occurs in the visual encoding of spatial detail. Our focus was on the standard visual parameter, SF. We analyzed peak or preferred SF levels, bandwidth or tuning characteristics, and high SF cutoff values. Previous physiological and behavioral demonstrations have shown that SF and other visual stimulus variables follow a coarse-to-fine process (e.g. Ringach *et al.*, 1997; Mazer *et al.*, 2002; Allen & Freeman, 2006). Similar processing sequences have also been demonstrated in auditory, somatosensory, and motor systems as noted above (see Introduction), suggesting a general neural coding strategy. Although original studies had suggested that this is a cortical process, we previously demonstrated it for neurons in the LGN (Allen & Freeman, 2006). As an obvious speculation is that the process begins at an earlier stage of visual processing, i.e. the retina, we first sought to establish this from recordings of retinal ganglion cells. Once we confirmed that the coarse-to-fine sequence begins at the retina, we next compared characteristics of the process between the retina and LGN. This comparison was facilitated by part of our neuronal sample, which consisted of pairs of retina and LGN cells that are monosynaptically connected. Finally, we examined potential mechanisms of coarse-to-fine processing by analysis of center-surround RF characteristics. Based on previous studies (Kuffler, 1953; Hubel & Wiesel, 1961), we expected an accentuated coarse-to-fine process in the LGN compared with that in the retina.

Our detailed analysis of spatiotemporal RF properties shows, for both the retina and LGN, that there are temporal shifts in peak or preferred and cutoff SF and tuning bandwidth changes that are correlated with temporal delays between center and surround RF regions. The temporal delay is positively correlated with shifts in SF. The longer the delay, the greater is the shift in SF. For tuning bandwidth, the inverse or negative correlation is observed. Longer delays are correlated with narrower bandwidths. As there are clear differences for both the retina and LGN in temporal latencies of center and surround RF components, peak response strengths for these subregions vary. To determine how temporal differences in subregion response strength are related to SF peak and bandwidth values, we

calculated the latencies at which center and surround RF strengths are equal. The results in Fig. 7D and E show clear patterns for both retina and LGN cells of both X and Y types. Nearly all data fall above the Y=X line showing that there is a consistent short delay (around 10 ms) between balanced center-surround response strengths and peak SF values. Bandwidth reduction has a similar relationship with a slightly shorter lag (around 5 ms). These data demonstrate that peak SF values are attained during a dominant period of center RF response and close to a time-point when center and surround strengths are equal.

The differences in temporal activation of center and surround RF regions that we observed here have also been noted in previous studies of both the retina and LGN (Kuffler, 1953; Hubel & Wiesel, 1961; Enroth-Cugell *et al.*, 1983; Dawis *et al.*, 1984; Cai *et al.*, 1997; Usrey *et al.*, 1999). In general, surround RF regions are temporally delayed with respect to centers. This applies to the ON or OFF center and X and Y RF types. We note in the current study that center-surround temporal response differences are correlated with coarse-to-fine processing. If the correlation is also functional, the magnitude of this tuning spatial sequence should be proportional to the temporal differences between center and surround RF responses. Our data are consistent with this notion, i.e. greater coarse-to-fine dynamics are correlated with larger time differences between center and surround responses. Again, there are no obvious differences between the ON and OFF center RF categories, X or Y types, or retina and LGN. As the source of coarse-to-fine tuning begins in the retina, it is clearly relevant to consider the process there that generates the effect. Although functional connections between retinal cones and ganglion cells have been studied, there appears to be no clear information concerning the roles of horizontal, bipolar, and amacrine cells in generating the coarse-to-fine processing of retinal ganglion cells (Baylor *et al.*, 1971a,b; Flores-Herr *et al.*, 2001).

Previous reports of the physiological characteristics of RFs in the retina and LGN indicate differences between these two regions. Specifically, peak or preferred and cutoff SF values, and center-surround interaction in the LGN were considered to be stronger than those in the retina (e.g. Enroth-Cugell et al., 1983; Cai et al., 1997). In the current study, we anticipated that this difference would be expressed in the coarse-to-fine spatial processing domain. Our sample of monosynaptically connected cell pairs in the retina and LGN provides a unique opportunity to examine this expectation. For the connected cell pairs, and also the independent populations of retinal and LGN cells, our data show that the mean peak and cutoff SF values are higher in the LGN compared with the retina. However, we do not find differences in magnitudes or temporal characteristics of coarse-to-fine dynamics in either connected or independent retina and LGN cell populations. Considered together, coarse-to-fine tuning begins in the retina at relatively lower SF values and progresses to higher SF levels in the LGN and then the visual cortex. This constitutes a rapid temporal cascade of spatial information that proceeds from lower to higher SF values in early and then central neurons in the visual pathway.

Acknowledgments

This research was supported by NIH Grants EY01175 and EY013588.

Abbreviations

LGN	lateral geniculate nucleus
RF	receptive field
SF	spatial frequency

REFERENCES

Allen EA, Freeman RD. Dynamic spatial processing originates in early visual pathways. J Neurosci. 2006; 26:11763–11774. [PubMed: 17093097]

Baylor DA, Fuortes MG, O'Bryan PM. Lateral interaction between vertebrate photoreceptors. Vision Res. 1971a; 11:1195–1196. [PubMed: 5156791]

Baylor DA, Fuortes MG, O'Bryan PM. Receptive fields of cones in the retina of the turtle. J Physiol. 1971b; 214:265–294. [PubMed: 5579638]

Bredfeldt CE, Ringach DL. Dynamics of spatial frequency tuning in macaque V1. J Neurosci. 2002; 22:1976–1984. [PubMed: 11880528]

Cai D, DeAngelis GC, Freeman RD. Spatiotemporal receptive field organization in the lateral geniculate nucleus of cats and kittens. J Neurophysiol. 1997; 78:1045–1061. [PubMed: 9307134]

Dawis S, Shapley R, Kaplan E, Tranchina D. The receptive field organization of X-cells in the cat: spatiotemporal coupling and asymmetry. Vision Res. 1984; 24:549–564. [PubMed: 6740975]

DeAngelis GC, Ohzawa I, Freeman RD. Spatiotemporal organization of simple-cell receptive fields in the cat's striate cortex. I. General characteristics and postnatal development. J Neurophysiol. 1993a; 69:1091–1117. [PubMed: 8492151]

DeAngelis GC, Ohzawa I, Freeman RD. Spatiotemporal organization of simple-cell receptive fields in the cat's striate cortex. II. Linearity of temporal and spatial summation. J Neurophysiol. 1993b; 69:1118–1135. [PubMed: 8492152]

Enroth-Cugell C, Robson JG, Schweitzer-Tong DE, Watson AB. Spatio-temporal interactions in cat retinal ganglion cells showing linear spatial summation. J Physiol. 1983; 341:279–307. [PubMed: 6620181]

Flores-Herr N, Protti DA, Wassle H. Synaptic currents generating the inhibitory surround of ganglion cells in the mammalian retina. J Neurosci. 2001; 21:4852–4863. [PubMed: 11425912]

Hegde J. Time course of visual perception: coarse-to-fine processing and beyond. Prog Neurobiol. 2008; 84:405–439. [PubMed: 17976895]

Hubel DH, Wiesel TN. Integrative action in the cat's lateral geniculate body. J Physiology. 1961; 155:385–398.

Jones JP, Palmer LA. The two-dimensional spatial structure of simple receptive fields in cat striate cortex. J Neurophysiol. 1987; 58:1187–1211. [PubMed: 3437330]

Jones JP, Stepnoski A, Palmer LA. The two-dimensional spectral structure of simple receptive fields in cat striate cortex. J Neurophysiol. 1987; 58:1212–1232. [PubMed: 3437331]

Kuffler SW. Discharge patterns and functional organization of mammalian retina. J Neurophysiol. 1953; 16:37–68. [PubMed: 13035466]

Levick WR, Cleland BG, Dubin MW. Lateral geniculate neurons of cat: retinal inputs and physiology. Invest Ophthalmol. 1972; 11:302–311. [PubMed: 5028229]

Linsenmeier RA, Frishman LJ, Jakiela HG, Enroth-Cugell C. Receptive field properties of x and y cells in the cat retina derived from contrast sensitivity measurements. Vision Res. 1982; 22:1173–1183. [PubMed: 7147728]

Marr, D. A computational investigation into the human representation and processing of visual information. W.H. Freeman and Co.; 1982.

Mastronarde DN. Two classes of single-input X-cells in cat lateral geniculate nucleus. I. Receptive-field properties and classification of cells. J Neurophysiol. 1987a; 57:357–380. [PubMed: 3559684]

Mastronarde DN. Two classes of single-input X-cells in cat lateral geniculate nucleus. II. Retinal inputs and the generation of receptive-field properties. J Neurophysiol. 1987b; 57:381–413. [PubMed: 3559685]

Mazer JA, Vinje WE, McDermott J, Schiller PH, Gallant JL. Spatial frequency and orientation tuning dynamics in area V1. Proc Natl Acad Sci U.S.A. 2002; 99:1645–1650. [PubMed: 11818532]

McSorley E, Findlay JM. An examination of a temporal anisotropy in the visual integration of spatial frequencies. Perception. 1999; 28:1031–1050. [PubMed: 10664752]

Menz MD, Freeman RD. Stereoscopic depth processing in the visual cortex: a coarse-to-fine mechanism. Nat Neurosci. 2003; 6:59–65. [PubMed: 12469131]

Nishimoto S, Arai M, Ohzawa I. Accuracy of subspace mapping of spatiotemporal frequency domain visual receptive fields. J Neurophysiol. 2005; 93:3524–3536. [PubMed: 15647396]

Over EA, Hooge IT, Vlaskamp BN, Erkelens CJ. Coarse-to-fine eye movement strategy in visual search. Vision Res. 2007; 47:2272–2280. [PubMed: 17617434]

Pack CC, Born RT. Temporal dynamics of a neural solution to the aperture problem in visual area MT of macaque brain. Nature. 2001; 409:1040–1042. [PubMed: 11234012]

Rathbun DL, Warland DK, Usrey WM. Spike timing and information transmission at retinogeniculate synapses. J Neurosci. 2010; 30:13558–13566. [PubMed: 20943897]

Reid RC, Alonso JM. Specificity of monosynaptic connections from thalamus to visual cortex. Nature. 1995; 378:281–284. [PubMed: 7477347]

Reid RC, Victor JD, Shapley RM. The use of m-sequences in the analysis of visual neurons: linear receptive field properties. Vis Neurosci. 1997; 14:1015–1027. [PubMed: 9447685]

Ringach DL, Hawken MJ, Shapley R. Dynamics of orientation tuning in macaque primary visual cortex. Nature. 1997; 387:281–284. [PubMed: 9153392]

Ruksenas O, Fjeld IT, Heggelund P. Spatial summation and center-surround antagonism in the receptive field of single units in the dorsal lateral geniculate nucleus of cat: comparison with retinal input. Vis Neurosci. 2000; 17:855–870. [PubMed: 11193102]

Shapley R, Hawken M, Ringach DL. Dynamics of orientation selectivity in the primary visual cortex and the importance of cortical inhibition. Neuron. 2003; 38:689–699. [PubMed: 12797955]

Sripati AP, Yoshioka T, Denchev P, Hsiao SS, Johnson KO. Spatiotemporal receptive fields of peripheral afferents and cortical area 3b and 1 neurons in the primate somatosensory system. J Neurosci. 2006; 26:2101–2114. [PubMed: 16481443]

Sutter, E. A practical non-stochastic approach to linear time-domain analysis. In: v, m, editor. Advanced methods of physiological systems modeling. Los Angeles: University of Southern California; 1987. p. 303-315.

Usrey WM, Reid RC. Synchronous activity in the visual system. Annu Rev Physiol. 1999; 61:435–456. [PubMed: 10099696]

Usrey WM, Reppas JB, Reid RC. Paired-spike interactions and synaptic efficacy of retinal inputs to the thalamus. Nature. 1998; 395:384–387. [PubMed: 9759728]

Usrey WM, Reppas JB, Reid RC. Specificity and strength of retinogeniculate connections. J Neurophysiol. 1999; 82:3527–3540. [PubMed: 10601479]

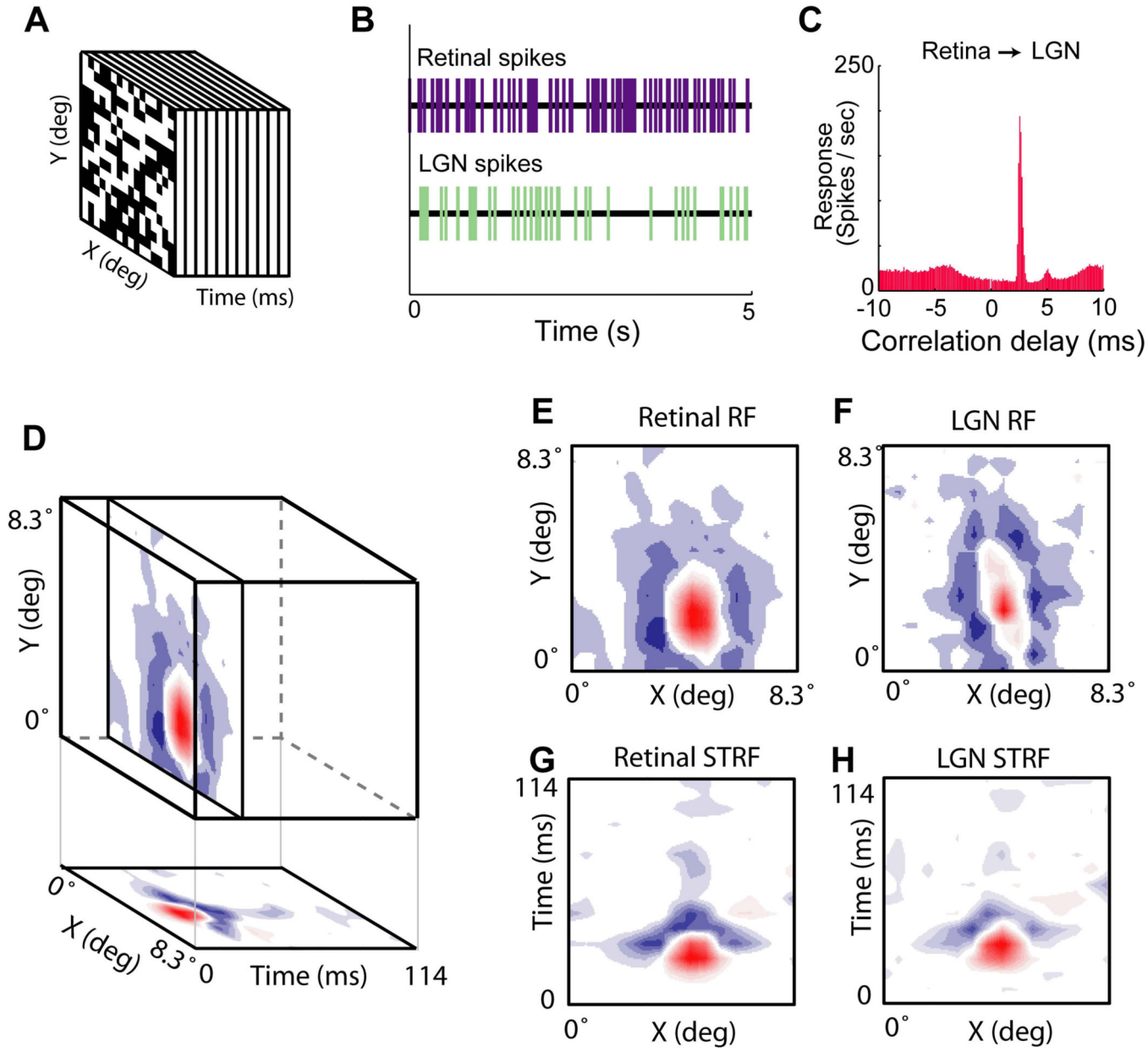

Fig. 1.

Measurement of spatiotemporal RFs from pairs of monosynaptically connected retinal ganglion cells and LGN neurons. (A) A spatiotemporal three-dimensional RF map. (B) Concurrent spike trains from ganglion and LGN cells. (C) A cross-correlogram between simultaneously recorded neurons in the retina and LGN. (D) Three-dimensional spatiotemporal RF for an ON-center retinal ganglion cell. Red is ON or bright excitatory and blue is OFF or dark excitatory. (E and F) X,Y spatial RFs for synaptically coupled retinal and LGN cells. (G and H) XT spatiotemporal RFs for the same pair of cells as in E and F.

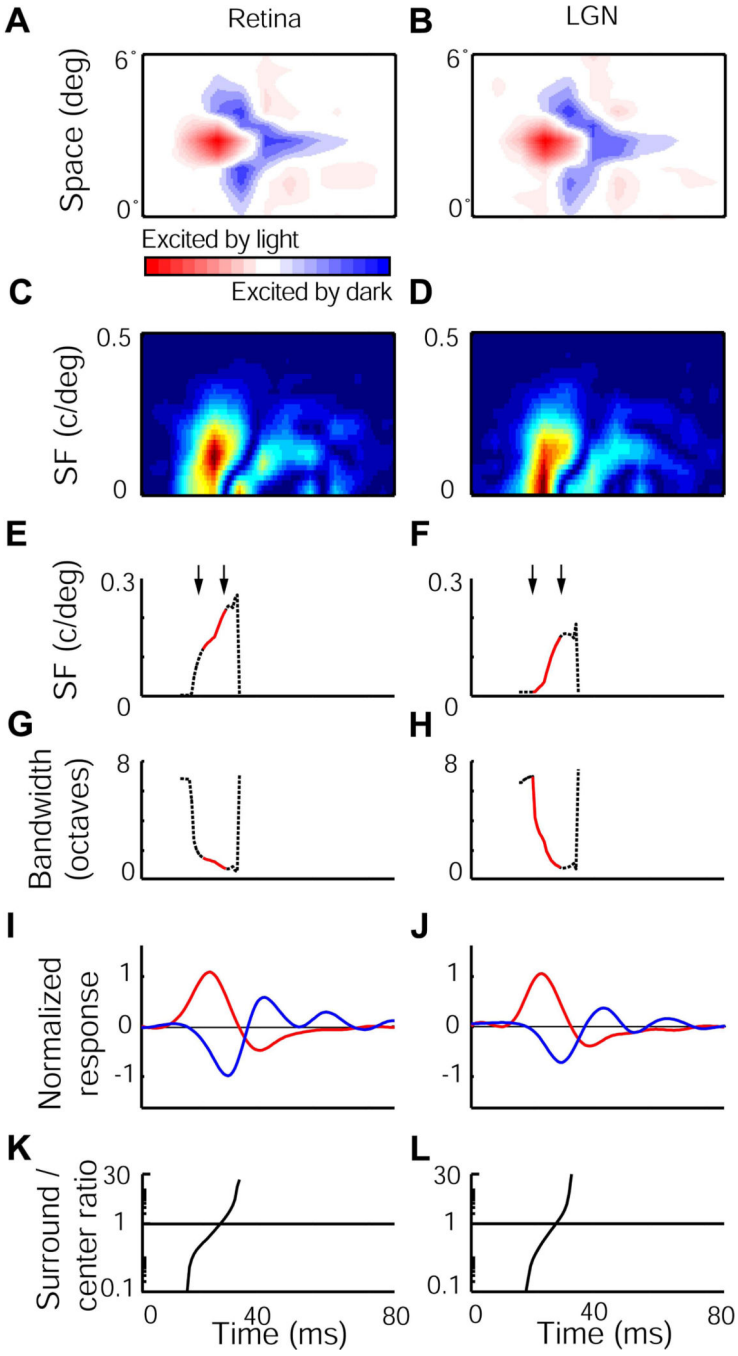

Fig. 2.

Pair of synaptically coupled neurons from the retina (ganglion cell) and LGN. (A and B) ON-center spatiotemporal RFs. (C and D) Spectrotemporal RF dynamics for the cell pair in A and B. (E and F) Changes in peak SF. Peak SFs within intervals in red and indicated temporally by pairs of downward arrows. (G and H) Change in bandwidth for the same interval as in E and F. (I and J) Impulse responses for the cell pair. RF center subunit ON response (red) and RF surround OFF response (blue). (K and L) Ratios of relative surround over center RF strengths.

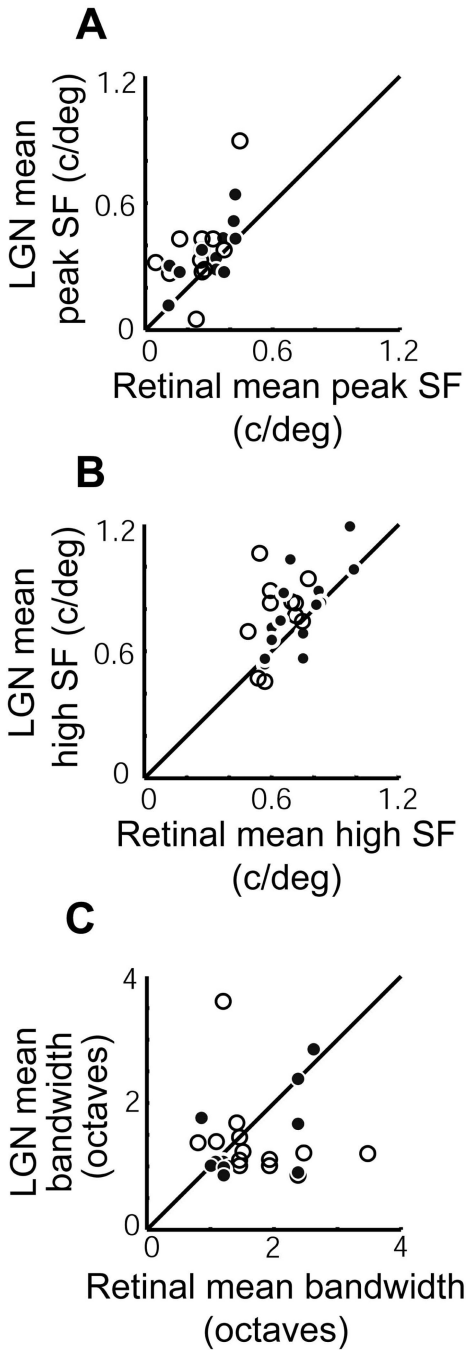

Fig. 3.

SF peaks (preferred levels), high SF cutoffs, and selectivity for connected pairs of retina and LGN cells. (A) Mean peak SF values for cells with relatively strong (connection strengths above the population median; filled circles) or weak (connection strengths below the population median; open circles) connection correlation strengths. (B) Similar to A, data are shown for high SF cutoff values for retina and LGN neurons. (C) Mean bandwidth values for the retina and LGN.

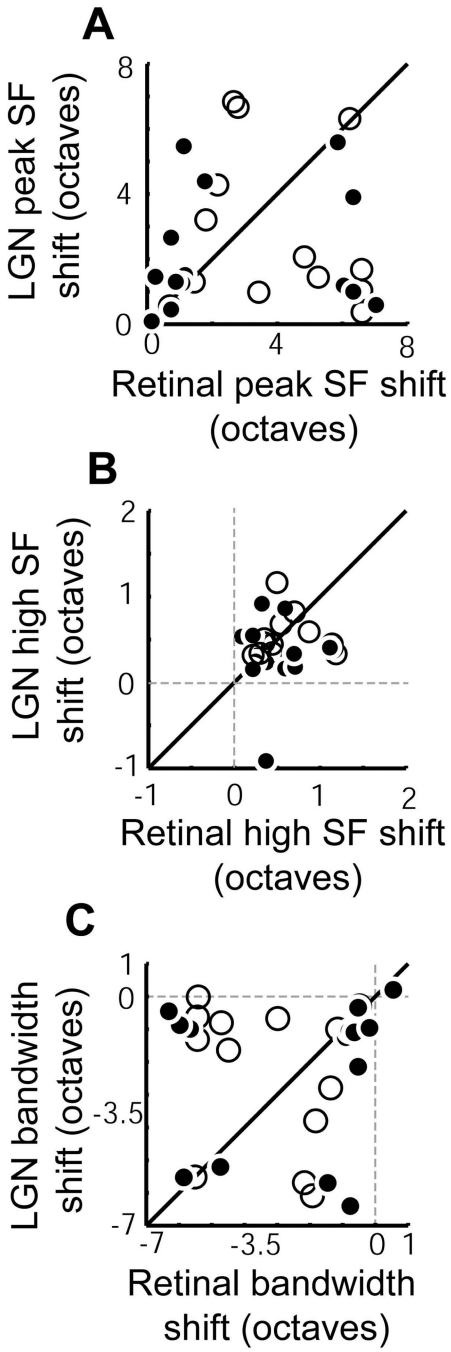

Fig. 4.

Dynamic shifts in SF peaks and high SF cutoff values for pairs of coupled cells from the retina and LGN. As in Fig. 3, relatively strong and weak intercellular connections are represented by filled and open circles, respectively. (A) Positive spatial shifts in peak SF values are shown for retina and LGN cells. (B) Similar positive dynamic shifts are depicted for high SF cutoffs for the retina and LGN. (C) Negative shifts in SF tuning bandwidths indicate increased SF selectivity for the retina and LGN.

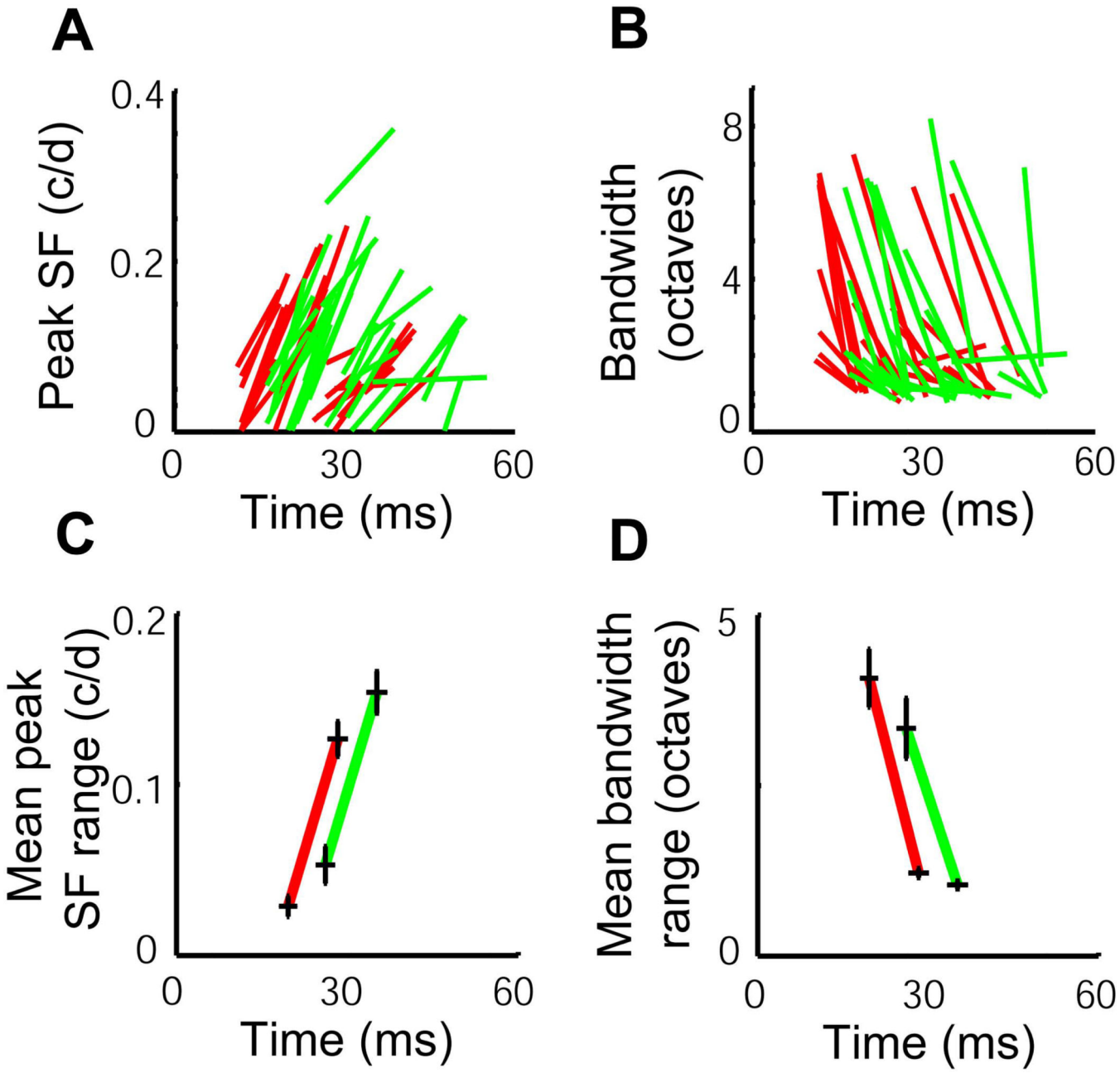

Fig. 5.

Temporal changes in SF peak and selectivity levels for connected cell pairs (n=27). (A) Peak SF changes as a function of time. Initial and final SF levels are depicted by the end-points of each red (retina) and green (LGN) line. Slopes of lines indicate rates of the coarse-to-fine dynamic. All lines slant to the right, indicating positive peak SF changes over time. (B) Tuning width changes for the same cells as shown in A. (C) Mean peak SF ranges are depicted for initial and final time-points. (D) Mean bandwidth ranges are shown that parallel those of peak SF range changes.

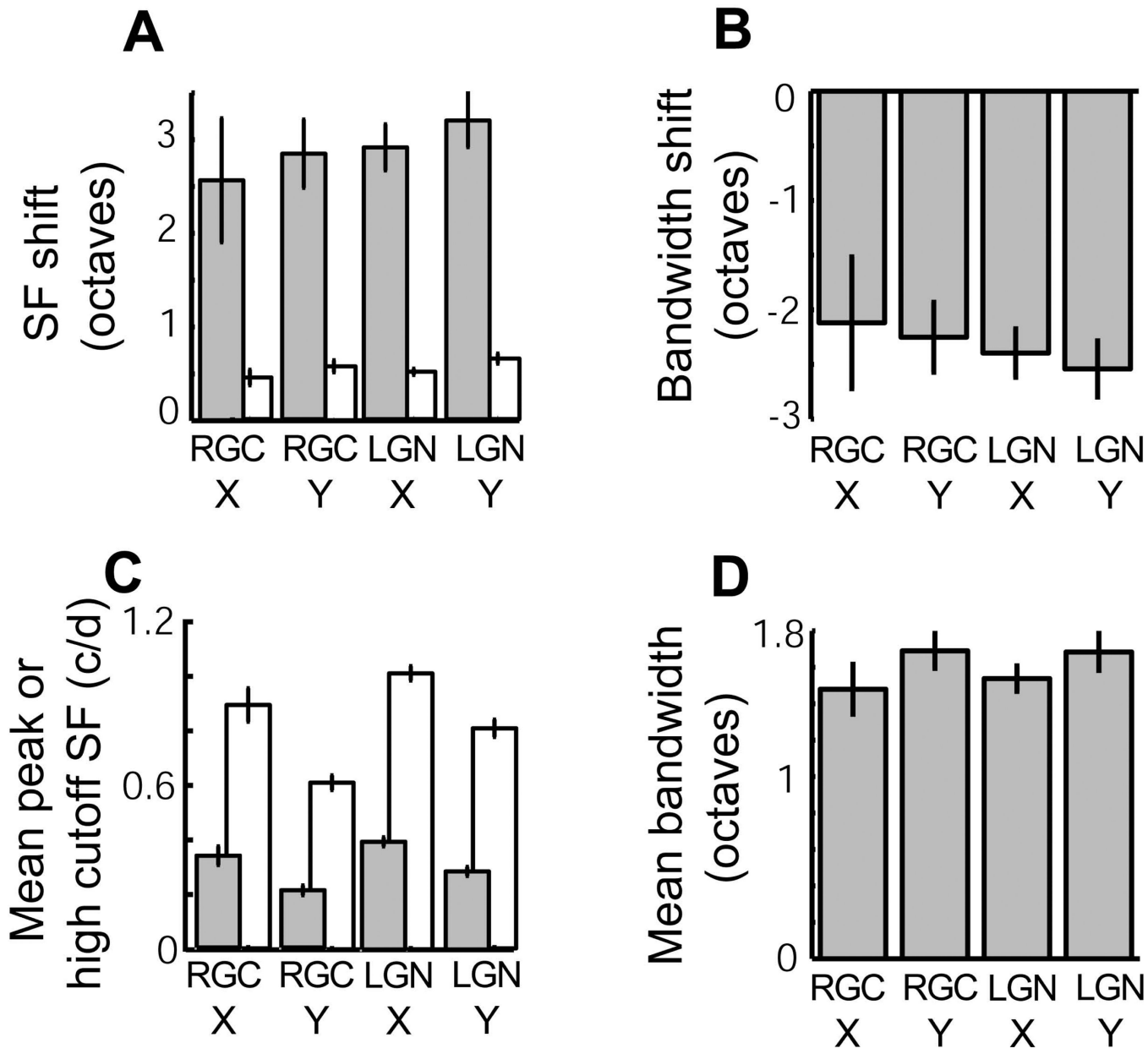

Fig. 6.

Summaries for peak and high cutoff SF means and shifts for the entire population of connected and separate RGCs and LGN neurons (total n=243; RGCs: n=52, 13 X cells, 29 Y cells; LGN neurons: n=191, 118 X cells, 73 Y cells). (A) Peak (shaded bars) and high cutoff (open bars) shifts in SF for X and Y cells. (B) SF tuning characteristics in bandwidth shifts for the same four categories as in A. (C) Mean peak or high cutoff SF values (shaded and open bars, respectively) for the same four categories as A and B. LGN cells are clearly higher in mean SF values for both X and Y categories. X cells exhibit higher mean SF values than Y cells. The same trend occurs for high SF cutoffs (open bars). (D) Mean bandwidths for the same four categories as in A-C.

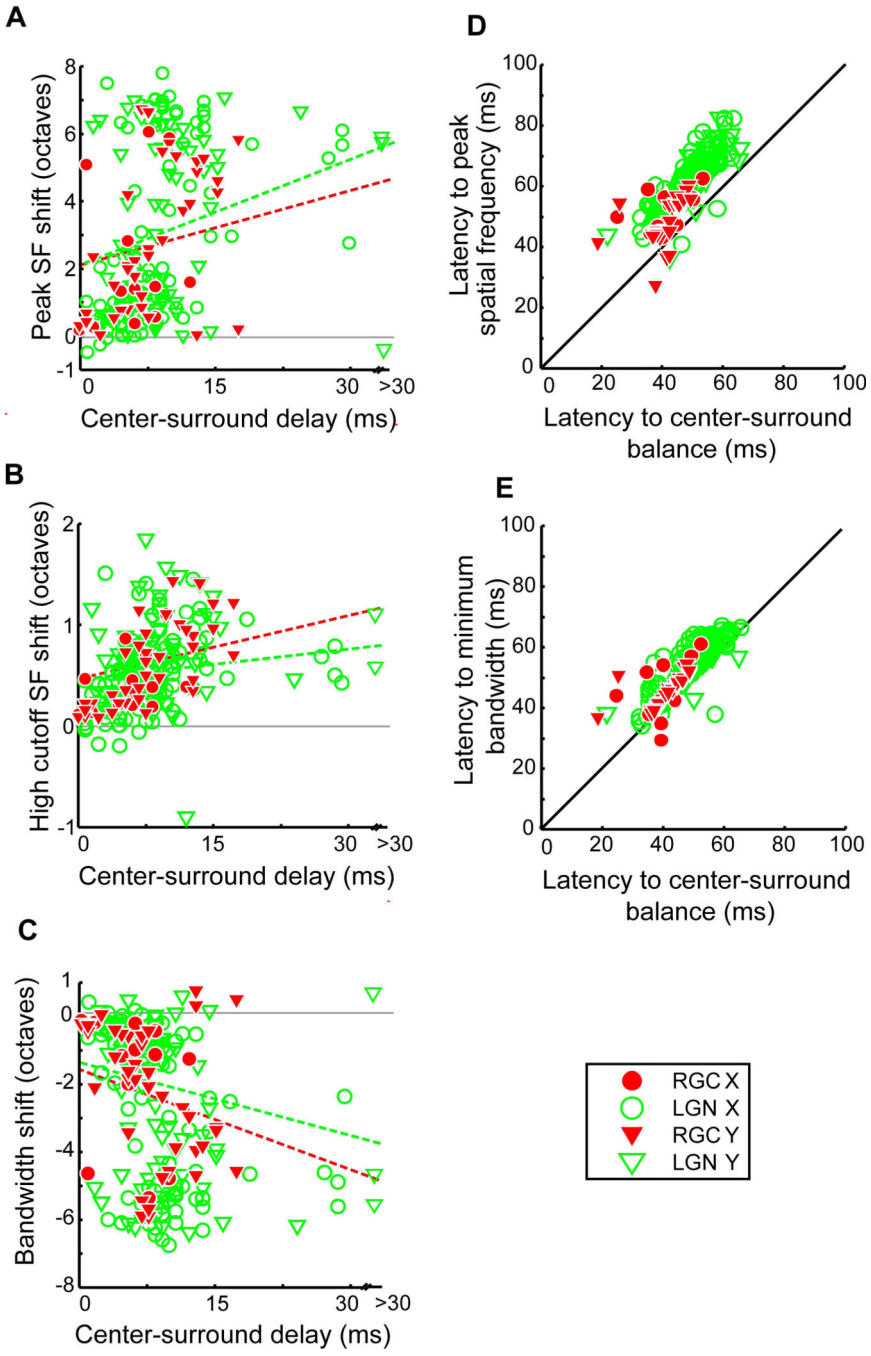

Fig. 7.

Temporal differences for SF parameters between center and surround RF components across the sample of RGCs and LGN neurons. (A) Center-surround delay as a function of peak SF shift shows a weak positive but statistically significant correlation. Sample size is the same as in Fig. 6. Dashed line is least-squares fit (r^2=0.091, $p<0.01$). X and Y type cells are indicated by circles and triangles, respectively. (B) Similar comparison between center-surround delay and high cutoff SF shift [as with A, a weak positive but statistically significant correlation (r^2=0.03, $p<0.01$)]. Dashed line is the least-squares fit to the data. (C) Center-surround delay as a function of bandwidth shift shows a bimodal distribution. Bandwidth shift is correlated with center-surround delay, i.e. longer delays with larger shifts in SF selectivity. Dashed line is the least-squares fit (r^2=0.090, $p<0.01$). (D)

Latency to center-surround balance vs. latency to peak SF (n=226 cells; RGCs: n=13 X cells, 37 Y cells; LGN cells: n=105 X cells, 71 Y cells; NB 17 cells were excluded in this analysis from the total sample of 243 cells, as they did not achieve center/surround balance within the analysis window described in Materials and Methods). Abscissa is latencies to times at which center and surround RF subunits have balanced strengths. Ordinate is latencies to highest SF peak. There is a clear positive correlation with nearly all data points above the unity line. Therefore, peak SF values occur slightly after center and surround subunits have equal strengths. (E) Similar comparison of bandwidth selectivity for the same cells as shown in D. There is a clear positive correlation again between the two variables. Cells again are mainly above the Y = X line.